Rational enhancement of nanobiotechnological device functions illustrated by partial optimization of a protein-sensing field effect transistor

T R Nicholson III[1], S Gupta[1], X Wen[2], H-H Wu[2], R Anisha[2], P Casal[1], K J Kwak[3], B Bhushan[3], P R Berger[2,4], W Lu[2], L J Brillson[2,4], and **S C Lee[1,5,6]***

[1] Department of Biomedical Engineering, The Ohio State University, Columbus, Ohio, USA
[2] Department of Electrical and Computer Engineering, The Ohio State University, Columbus, Ohio, USA
[3] Department of Mechanical Engineering, The Ohio State University, Columbus, Ohio, USA
[4] Department of Physics, The Ohio State University, Columbus, Ohio, USA
[5] Department of Chemical and Biomolecular Engineering, The Ohio State University, Columbus, Ohio, USA
[6] The Davis Heart and Lung Research Insititute, The Ohio State University, Columbus, Ohio, USA

The manuscript was received on 14 June 2010 and was accepted after revision for publication on 03 September 2010.

DOI: 10.1243/17403499JNN184

Abstract: Semiconductor field effect transistors (FETs) are widely used as biosensors, although a potentially powerful application of FET sensing technology (planar immunoFETs sensing proteins at physiological salt concentrations) has long been argued to be intrinsically infeasible. The infeasibility assessment has come under increasing scrutiny of late, and has been found to be lacking on conceptual and empirical grounds. This paper summarizes some, but, by no means all, of the strategies that have been pursued to render the use of immunoFETs, and analogous FET sensors that detect the electrical fields of proteins bound to affinity elements on FET sensing channels (protein-sensing bioFETs), practical in high-salt biological buffers. This paper provides original characterization of oxidized AlGaN surfaces and interfacial polymer/protein films of protein-sensing AlGaN/GaN HFETs. It shows those films to influence significantly FET sensitivity/signal accumulation. The data indicate that re-assessment of the classical assertion of immunoFET infeasibility is long overdue. Beyond substantiating the feasibility of immunoFET operation under solution conditions as found *in vivo*, data presented here also suggest that transition away from costly AlGaN/GaN HFETs to inexpensive silicon-based immunoMOSFETs may be possible. If so, immunoFETs, dismissed as infeasible 20 years ago, may yet become powerful clinical tools.

Keywords: immunoFET, protein detection, physiological salt concentrations, AlGaN/GaN

1 INTRODUCTION

Semiconductor field effect transistors (FETs) are three terminal devices in which the current between source and drain terminals (I_{sd}) in the semiconductor channel is modulated by the presence of proximal electrical fields (Fig. 1). This 'gating' effect can be mediated by a gate electrode, which is insulated from the semiconductor channel by a dielectric layer, and to which a bias is applied, or by the presence of charged molecules proximal to the channel dielectric. This latter mode of gating has allowed the development of FET-based sensors to detect ions, gases, and biological macromolecules [**1**] (Fig. 1).

FET sensors detecting ions (isFETs), nucleic acids (genFETs), products of enzymatic reactions (enFETs), and cells (cellFETs) are widely accepted [**1**]. Direct detection of proteins by planar FET is potentially as attractive as these other FET sensing modalities as it requires no secondary reagents, offers real-time

**Corresponding author: Department of Molecular and Cellular Biochemistry, The Ohio State University, 473 West 12th Avenue, Columbus OH 43210, USA*
email: Stephen.Lee@osumc.edu; lee.1996@osu.edu; lee-29@medctr.osu.edu

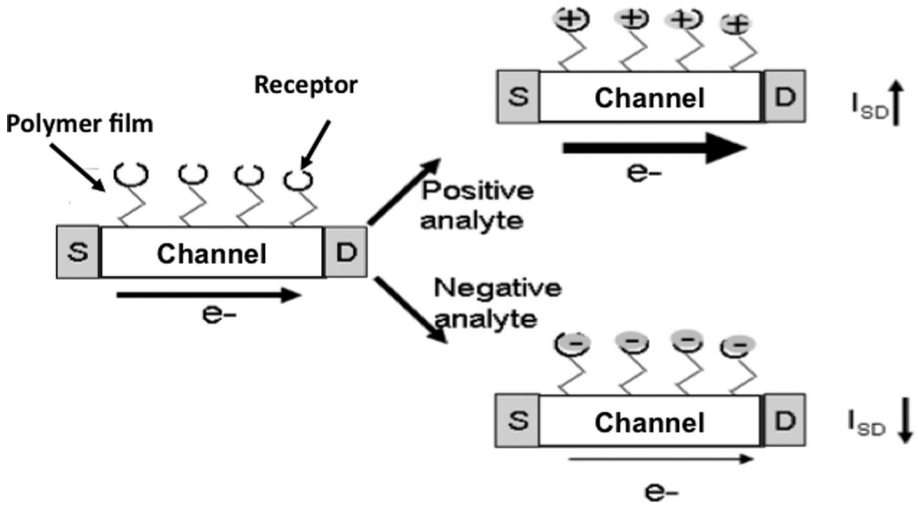

Fig. 1 Current (I_{SD}) responses of an n-type immunoFET to binding of oppositely charged protein analytes to receptors on the FET sensing channel. Source (S) and drain (D) contacts are indicated

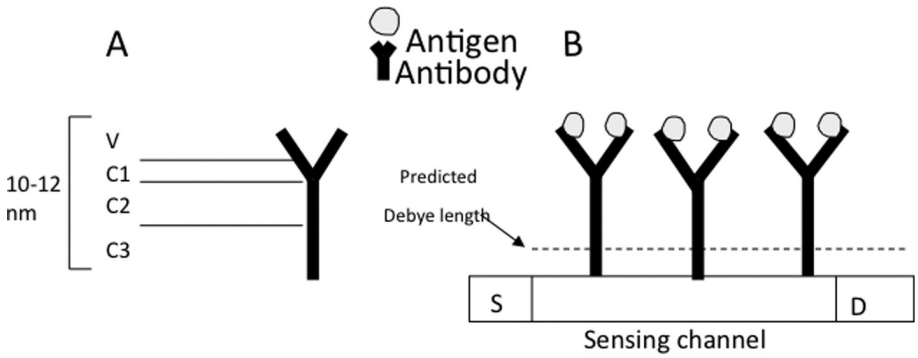

Fig. 2 Artist's conception (factually inaccurate, see text) of antibody on an immunoFET sensing channel. (a) Antibody domains (constant 1, 2, 3 indicated as C1, C2, C3 and variable as V) are shown; as is predicted Debye length in physiological buffer (150 mM salt 1–2 nm). (b) FET shown with the traditional (but scientifically inaccurate, see text) depiction of antibodies on FET sensing channels. Current source (S) and drain (D) are indicated. This flawed representation is central to the classical objection to the feasibility of immunoFETs (from Shapiro *et al.*, 2007 [**6**] after Schöning and Pohgossian [**1**])

detection with a scalable/tunable device architecture, leading to significant economies of cost and labour relative to other protein detection methods. Unfortunately, the feasibility of FETs using antibodies (or derivatives thereof) to localize charged protein analytes to FET channel surfaces for electrical detection (immunoFETs) is controversial.

Use of immunoFETs to detect physiological concentrations of protein analytes in physiological buffers (150 mM salt) has been assessed to be infeasible [**1**–**5**], based on the (inaccurate) schematic representation of immunoFETs of Fig. 2. The critical flaws in classical immunoFET feasibility assessment embodied in Fig. 2 concern antibody structural dynamics (antibodies are not rigid bodies) and adsorption of antibodies to surfaces (antibodies do not bind to surfaces exclusively at their C3 domain, contrary to the assumption of the classical model). The representation of antibody dynamics and adsorption embodied in the classical model is inaccurate and has been established science in immunology for more than 50 years [**7**, **8**].

Given the faulty assumptions supporting the classical assessment of immunoFET feasibility, it is not surprising that it is unable to account for FET sensing data from multiple groups using multiple device platforms [**6**, **9**–**15**], as Estrela and colleagues assert [**9**]. The issue of planar immunoFET feasibility/infeasibility is significant for the sensing opportunity that the classical assessment denies: inexpensive and convenient interrogation of specific protein content of tissue microenvironments in multiple disease states, among other applications. Adherence to the fundamentally flawed classical assessment of immunoFET feasibility [**3**] has precluded the development of immunoFET-based clinical tools for nearly 20 years.

The classical immunoFET assessment [**3**] correctly asserts that the FET sensor signal is inversely related to analyte charge distance from the FET sensing channel and that FET detection of electrical fields of protein analytes held at nanoscale distances from the FET channel are diminished in direct proportion to buffer ion concentration [**6**, **11**]. However, the classical assessment errs in its implicit assumption that protein and interfacial engineering cannot bring protein analyte charges into sufficient proximity to the sensing channel for FET detection. The assessment also ignores the possibility that FET hardware modifications (for instance, the use of so-called control gates to bias devices to the exponential subthreshold response regime [**16**]) might alter the minimal analyte concentrations or distances over which analyte electrical fields might be detected. Additional flaws include the consideration of analyte proteins as point charges, the assumption that antibody molecules (that serve as analyte receptors) are rigid, the failure to consider protein engineering approaches in selection/design of analyte receptors, as well as the scientifically inaccurate assumption that antibodies bind to surfaces by adsorption exclusively at a single region of the antibody (the antibody C3 domain, see Fig. 2) [**6**, **10**, **11**].

Multiple investigators have observed [**6**, **9–15**, **17**, **18**] that the classical infeasibility assessment could not accurately describe immunoFET structure and behaviour, even at its inception in 1991. Aside from empirical evidence of the feasibility of immunoFET sensing in biological environments [**6**, **9–15**, **17**, **18**], the flaws of the classical infeasibility assessment [**6**, **10**, **11**] are conceptual and fundamental [**6**, **11**]. The classical assessment can provide no significant insight into the mechanism, should it be the case that immunoFETs prove infeasible in biologic buffers. However, the fact is that immunoFETs and analogous protein-sensing bioFETs can indeed function sensitively in biologic osmolarity environments, as data summarized in Fig. 3, and corroborated by multiple independent studies show [**6**, **9–15**, **17**, **18**]. Nonetheless, current protein-sensing FET technology is not ready for immediate clinical translation, and the classical assessment has genuine utility in its implicit identification of challenges to device optimization that might be addressed by micro/nanoscale solutions.

Remediation of the limitations of current immunoFETs might be approached through molecular engineering of nanoscale components (antibody-based receptors, choice of analyte epitopes recognized by antibody receptors, interfacial polymeric film dimensions, etc.). Changes in FET hardware (use of one-dimensional (1D) sensing channel architectures, biasing the device to the threshold regime with a control gate, passivation against ion permeation by deposition of high-K dielectrics, etc.) might also offer approaches to enhanced immunoFET performance and sensitivity *in vivo*. For purposes of optimization, immunoFET sensors can be considered as integrated wholes, wherein suitability of some individual nanoscale components can be most productively considered in the context of other individual immunoFET components. For instance, analyte geometry, charge, and epitope distribution could potentially render some receptors or interfacial polymer films less suitable for use together in a single immunoFET than they are individually. ImmunoFET sensors thus represent nanosystems, whose realization may benefit from system-level design approaches [**19**, **20**].

This paper revisits earlier discussions of potential approaches to immunoFET optimization [**6**, **10**, **11**]. In the work described, immunoFET optimization has been informed by systems engineering perspectives, and multiple distinct levels of optimization have been pursued concurrently (Fig. 4). Based on the data

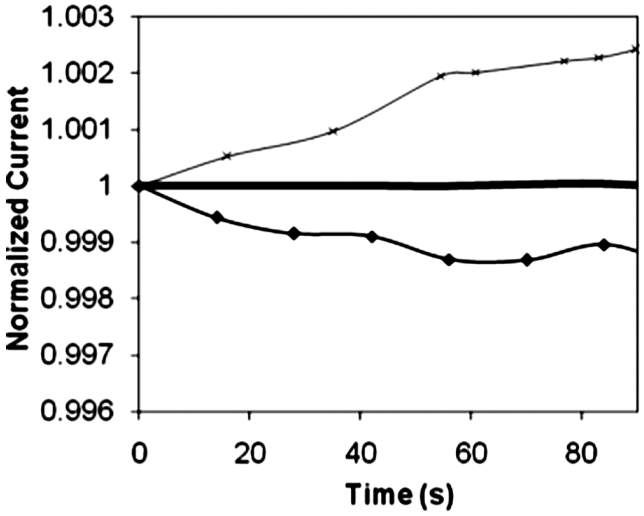

Fig. 3 Normalized, differential response of n-type HFET to charged (positive, negative) analytes. Biotinylated APTES layers were deposited on HFETs that were then treated with negatively charged streptavidin, producing the response shown by '-♦-'. After streptavidin treatment, devices were treated with positively charged biotinylated MIG, producing the responses indicated by '-X-'. Note that these curves are composed of hundreds of data points, and that -♦- and -X- do represent the individual data points that comprise the response curves, but are used to differentiate lines showing the streptavidin response curve and biotinylated MIG response curve, respectively. Negative controls verified that specific binding to the interface was required to produce a sensor signal. Negative controls are represented by the flat line between streptavidin and biotinylated MIG response curves. Raw data available in, and this figure adapted from, Gupta *et al.* [**11**]

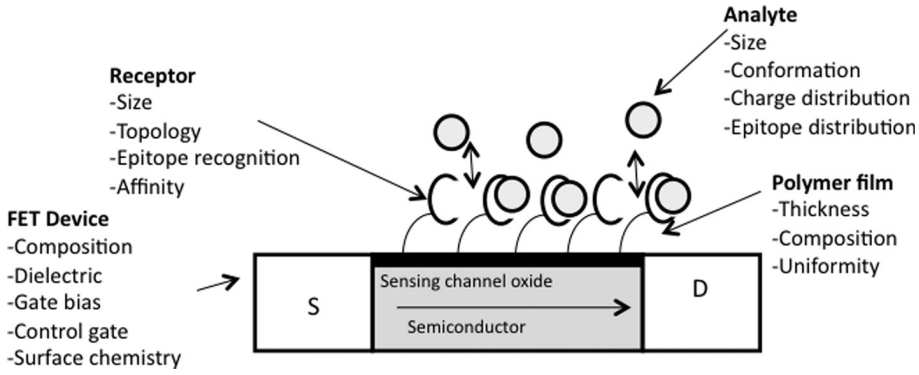

Fig. 4 Parameters that might influence immunoFET sensitivity to analyte and device cost

presented/summarized here, and data produced by multiple other investigators [**6**, **9**–**15**, **17**, **18**], the classical assessment would seem to be in the process of being overturned. Assuming that outcome, it seems likely that planar immunoFETs and similar protein-sensing FETs will find numerous applications *in vivo* and *ex vivo*, and may well become widely used in medicine, biotechnology, environmental remediation, and homeland defense.

2 MATERIALS AND METHODS

2.1 AlGaN device fabrication

AlGaN (aluminium gallium nitride) HFET devices were fabricated by previously established protocols [**6**, **11**]. Briefly, AlGaN/GaN heterostructures were purchased from CREE, Inc. (Raleigh, NC) and oxidized via oxygen plasma. Devices were designed and fabricated to accommodate and enable sensing under solution. Ohmic contacts consisted of titanium/aluminium/molybdenum/gold (Ti/Al/Mo/Au) multilayers deposited via e-beam evaporation and lift-off. Contacts were annealed at 850 °C for 30 s in a rapid thermal annealing system. To encapsulate the source and drain contacts and prevent shorting by buffer solution, microreservoirs over the sensing active areas were made of silicone.

2.2 Silicon capacitor fabrication and characterization

The p-type-silicon (Si) substrate was cleaned with a standard Si wafer cleaning process followed by an hydrofluoric acid (HF) dip just prior to oxide deposition. A 100 nm thick high-K oxide was then deposited via atomic layer deposition (ALD, below). For the control sample, a 100 nm silicon dioxide (SiO_2) layer was thermally grown. A 15 nm/150 nm Ti/Au layer was deposited at the bottom and top metal contacts. The top metal dots used for this experiment are designed to allow penetration of sodium ion (Na^+) into the oxide by providing access holes, while still allowing capacitors to be characterized with standard probe stations.

2.3 Atomic layer deposition (ALD)

ALD is a precise thin film deposition technique to produce materials, usually metal oxides, with very controlled thicknesses and composition. It utilizes a self-limiting layer-by-layer growth technique with intermittent pulses of a metal containing organometallic precursor and an oxidant, usually water. The substrate is exposed to the precursor, which reacts with the surface until it becomes saturated and a full monolayer has been chemisorbed, preventing any further adsorption. The precursor is then purged and the next precursor (water) is exposed and reacted with the initial absorbed layer, depositing a second layer of atoms. This cycle is repeated to build a dielectric interface layer-by-layer. For aluminium oxide (Al_2O_3) deposition trimethyl aluminium ($Al(CH_3)_3$) and H_2O were used as precursors at a growth temperature of 300 °C.

2.4 Silane film deposition

Silane film depositions were performed as described, with the exception that the hydrochloric acid (HCl)–ethanol step [**11**, **21**–**23**] was replaced by deionized water boil to hydroxylate the surface oxide in preparation for silane film deposition. Silane films were then biotinylated using EZ-Link Sulfo-NHS(*N*-hydroxysulfosuccinimide)-Biotin (Pierce, Rockford, IL, USA) as described in the references [**11**, **21**–**23**].

2.5 AlGaN oxidation by inductively coupled plasma

Oxidation and functionalization of AlGaN/GaN heterostructures without degradation of their electronic properties is critical for HFET devices. Specific oxidation protocols are available elsewhere [**24**]. Here AlGaN surfaces are oxidized by an inductively coupled plasma (ICP) protocol. High ICP power is applied to produce the plasma, allowing the AlGaN surface to

be oxidized by contact with uncharged oxygen radicals without significant ion bombardment, making the ICP protocol comparable to a chemical oxidation in terms of the limited defects it is expected to induce in the AlGaN surface.

2.6 ELISA quantification of proteins bound to silane films

After biotinylation, silane films on AlGaN wafer fragments (chips) were rinsed three times in deionized water and put into individual vials containing 330 μl of a 470 nM solution of streptavidin-HRP (SA-HRP, Pierce, Rockford, IL, USA) in phosphate buffered saline (PBS). Chips were incubated in SA-HRP for 5, 10, 30, and 60 min, then rinsed in three times in PBS and transferred to new vials containing 200 μl o-phenylenediamine (OPD) solution prepared as directed by the manufacturer (Sigma, St Louis, MO, USA). After 20 min of incubation, the OPD solution was pipetted into wells of a 96-well ELISA plate containing 50 μl 3M H_2SO_4 (sulphuric acid). The absorbance at 490 nm of each well was measured. Absorbance was normalized to the surface area of each chip (i.e. absorbance units/area of chip).

2.7 X-ray photoelectron spectrometry (XPS)

XPS is a surface science technique to characterize atomic composition, chemical bonding, and depth distribution of elements within the outer few monolayers of a solid [**25**]. Incident X-rays are used to excite photoelectrons from individual atoms of solid surfaces, which are then collected via a spectrometer and photoelectron kinetic energy is determined, allowing the construction of the XPS spectrum from the photoelectron intensity versus kinetic energy data. Photoelectron kinetic energy (E_K) is related to the binding energy (E_B) of a specific atomic orbital ($E_K = h\nu - E_B$, where $h\nu$ is the incident photon energy). In turn, the core level energies are characteristic of distinct core levels of specific elements. Shifts in these energies around their characteristic values (i.e. chemical shifts) are indicative of differential local chemical environments. Surface sensitivity of XPS derives from the short scattering length of electrons within solids [**26**], typically 2–20 Å when excited with the AlKα line X-ray source ($h\nu = 1486.6$ eV) used here.

Only electrons that emerge from the solid without scattering retain their initial kinetic energy to provide core level information. The extremely short photoelectron 'escape depth' facilitates XPS measurement of composition and bonding as a function of depth within the outer few monolayers. The angle-resolved capability of the PHI VersaProbe (Physical Electronics, Inc., Chanhassen, MN, USA) was used to collect photoelectrons as a function of angle with respect to the overlayer-deposited surface. Photoelectrons collected from the surface at an angle Θ relative to the surface plane contribute to the XPS spectrum from depths $d = \lambda \sin\Theta$, where $\lambda \simeq 16$ Å is the electron scattering length for the N 1s core level at $E_K = 1089$ eV and the O 1s level at 955 eV [**26**]. The intensity of the substrate emissions (I_S) decreases from initial intensity I_0 with decreasing analyser collection angle Θ according to the Beer–Lambert relationship $I_S = I_0^* e^{-d/(\lambda \sin\Theta)}$. Thus at small Θ, the XPS spectrum becomes increasingly surface-sensitive. This angle-resolved XPS (AR-XPS) technique was used to measure (a) the composition of the plasma-oxidized AlGaN/GaN surface oxide layer, (b) the composition of the deposited APDMES, and (c) the deposited APTES layers versus depth.

2.8 Electrical characterizations of HFETs

HFET electrical characterization was performed by measuring source–drain current–voltage and current–time characteristics using an Agilent 4156C semiconductor parameter analyser at room temperature by exposing the functionalized microreservoir region to analyte solution [**6**, **11**].

3 RESULTS AND DISCUSSION

3.1 Oxides of AlGaN/GaN surfaces

Previously [**11**], AlGaN surfaces of the protein-detecting HFETs were oxidized by a wet chemical protocol to minimize the induction of defects in the AlGaN/GaN heterostructure. As described in section 2, an oxygen ICP method was used to oxidize AlGaN surfaces analysed here. Detailed oxidation protocols, and physical/chemical comparison of wet chemical and plasma oxidized AlGaN surfaces and of silane polymer films deposited on these surfaces can be found elsewhere [**24**, **27**]. The data from these XPS studies are congruent, and show, among other things, that in contrast to the original chemically oxidized AlGaN surfaces [**11**], Ga rather than Al oxides are more prevalent in ICP-oxidized AlGaN surfaces. These studies imply that while oxidized, sputter-coated aluminium may be a valid and economical model of chemically oxidized AlGaN surfaces (as used in Bhushan *et al.* [**28**]), it may not be an appropriate model of ICP-oxidized surfaces.

3.2 Organic components of protein-sensing FET interfaces

Moving away from the FET channel surface itself, the next critical component of the sensor is typically a polymeric film, often referred to as a SAM or self-assembled monolayer. 'SAM' is often a misnomer for interfacial polymeric films on FET devices (see below and reference [**28**]), but whatever the

actual film morphology, the interfacial polymer layer provides chemically specific linkage between FET channel surface oxides and analyte-specific receptors. The film layer also necessitates distance between analyte (and associated charges) and FET sensing channels. The distance may provide steric clearance for analyte binding [**10**], but may reduce FET sensitivity. From that standpoint, the use of any interfacial polymeric films in immunoFET can be questioned, but the films provide two distinct benefits. Proteins directly adsorbed to microfabricated surfaces often do not bind strongly to those surfaces [**21**], and may be conformationally distorted by binding to the synthetic surface [**29**]. Second, adsorbed proteins, in the absence of a specific affinity element for the micromachined surface at a consistent position in their structures, are not consistently oriented on the surface. Lack of consistent orientation may make consistent sensor responses elusive, and interfacial engineering to maximize sensor sensitivity difficult [**6**, **10**, **30**, **31**]. Both of these issues can be addressed with a well-ordered interfacial polymer layer. Still, comparisons of different interfacial films [**6**, **10**, **11**, **20–22**, **28**] show that the specific characteristics of interfacial films profoundly affect device wear properties, analyte binding kinetics, and FET sensitivity properties.

3.3 Interfacial silane film structures

Aminopropyltriethoxysilane (APTES) is an amine-terminated alkoxysilane molecule widely used for surface functionalization in biosensing applications [**6**, **11**, **32**]. APTES is attractive for its high reactivity with multiple metal oxides and the flexibility that its amine terminal groups offer for bioconjugation to receptor molecules. Ideally, APTES would form SAMs on FET sensing channels, although APTES deposited from liquid media frequently forms multi-layered interfaces [**33**]. Multilayering of liquid-deposited APTES has been previously observed on multiple micromachined surfaces (SiO_2, Al_2O_3 [**23**, **33**, **34**], AlGaN [**28**], Wu *et al.*, 2010 [**35**]). Multilayered APTES interfaces are the consequence of the multivalency of the siloxane groups of the APTES monomer, which allow the molecule to polymerize [**28**]. Polymerized APTES can form a networked interface which is not only thicker than expected, but also can be debrided from a micromachined surface by very minimal abrasive insult [**20–22**, **28**].

Unlike APTES, aminopropyldimethylethoxysilane (APDMES) is a monoalkoxy silane. APDMES reacts readily with surface oxides and presents a terminal amine group for subsequent functionalization as does APTES, but because APDMES contains only one alkoxy group per monomer, APDMES–APDMES conjugation produces dimers that cannot further react with sensor surface oxides. Consequently, APDMES surface films are thinner (approximating the summed bond lengths of APDMES) and smoother (more ordered) than are APTES films [**28**] (Table 1). APTES and APDMES film structures on metal oxide surfaces are shown in Fig. 5.

Table 1 Table comparing characteristics of APDMES and APTES interfaces

Characteristic	APTES	APDMES
Polymer film thickness [**24**]	2.4 nm	1.2 nm
Streptavidin detection limit	1 mg/mL	250 pg/mL
ELISA streptavidin saturation absorbance (normalized per unit area)	0.334 abs/mm^2	0.155 abs/mm^2
Time to biochemical saturation of streptavidin	>60 min	<10 min

A prominent difference between APTES and APDMES films is the expected difference between the depths at which Si would first be encountered moving from the outermost surface of the films. Si is expected closer to the outer surface in a polymerized interface, in polymerized APTES films than in APDMES films (Fig. 5). Furthermore, the fraction of the total elemental composition comprised by nitrogen at the outermost surface of the films is expected to be greater in the more ordered APDMES film interface than in polymerized APTES films (Fig. 5). APTES and APDMES films on AlGaN surfaces were studied using XPS-ARS, allowing characterization of elemental composition of the films deposited on ICP-oxidized AlGaN surfaces as a function of depth.

The AR-XPS measurements of APTES and APDMES at $\Theta = 10°$ provide compositions with the highest surface sensitivity whose relative concentrations provide significant information about silane film orientation. Table 2 presents the $\Theta = 10°$ AR-XPS results for the percentage compositions of each element within the stacked silane film–oxide–AlGaN/GaN surface layers. These are derived by normalizing the deconvolved peak areas with sensitivity factors unique to the PHI VersaProbe. APTES extends further from the surface than APDMES (Fig. 5, Table 2), so the attenuation of the substrate Ga and Al by APTES should be stronger (Table 2). Indeed, the Al, Ga, and N intensities decrease 29, 33, and 32 per cent more, respectively, for APTES than for APDMES. Observed differences in Ga and Al peak attenuation between APTES and APDMES films are congruent with the known propensity of APTES to polymerize, and with ellipsometry measurements and AFM estimates of APTES film heights on SiO_2 and Al_2O_3 surfaces [**28**].

Furthermore, if the structure of APTES films is similar to the model presented in Fig. 5 [**28**], APTES films should have very limited preferential orientation of N versus Si or O at the outermost layers of the films, whereas APDMES should exhibit a strong preferential orientation of the amine group above the Si and O.

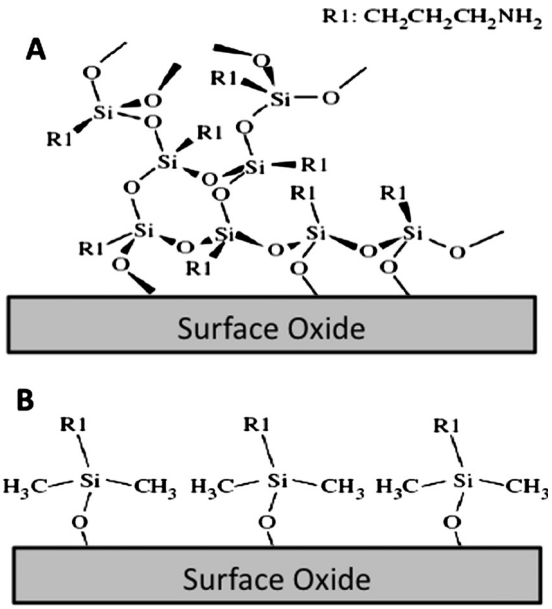

Fig. 5 Conceptual illustration of (a) APTES and (b) APDMES films deposited on metal oxide surfaces

Table 2 Percent compositions of elements within the stacked silane polymer film–oxide–AlGaN/GaN surface layers

SAM layer	Al 2p (%)	Ga 3d (%)	O 1s (%)	C 1s (%)	N 1s (%)	Si 2p (%)
APDMES	2.89	8.79	13.27	11.69	31.43	31.91
APTES	2.04	5.89	16.17	28.90	21.19	25.79

Hence, one expects a higher N versus Si I_{N1s}/I_{Si2p} and N versus O ratio I_{N1s}/I_{O1s} in APDMES versus APTES. Indeed, $I_{N1s}/I_{Si2p} = 0.98$ in APDMES is much higher than $I_{N1s}/I_{Si2p} = 0.82$ in APTES. Likewise, $I_{N1s}/I_{O1s} = 2.37$ is much higher in APDMES than $I_{N1s}/I_{O1s} = 1.31$ in APTES. The substantially higher I_{N1s}/I_{Si2p} and N versus O ratio I_{N1s}/I_{O1s} in APDMES versus APTES confirm the expected strong preferential orientation of the amine group above Si and O in APDMES films. These systematic variations suggest first that the hypothetical structure of APTES and APDMES films of Fig. 5 is valid to the extent that APDMES films are more strongly oriented (from the AlGaN surface outwards) siloxane bond to terminal amine than are APTES films deposited by the protocol used [**6**, **11**, **21**–**23**, **28**]. The results also demonstrate that the AR-XPS technique can be effective at distinguishing the molecular stacking sequences of other macromolecules (i.e. proteins) on semiconductor surfaces.

3.4 Summary of published validation of streptavidin and MIG sensing by HFET in physiological buffers

Contrary to the conclusion asserted by the classical assessment of FET protein sensor infeasibility in high-salt buffers [**1**–**5**], HFETs operated in physiological buffer (PBS, 150 mM in Na^+) can indeed detect protein analyte binding to AlGaN/GaN HFET sensing channels that have been derivatized with biotinylated polymer films [**6**, **11**]. This was completed with a model sensor exploiting streptavidin–biotin binding to represent antigen–antibody interaction. The streptavidin complex is within 2–3 fold the size of intact IgG antibodies, and larger than the smallest available antigen-binding competent antibody fragments (such as single chain fragment variable and single domain antibodies [**36**–**38**]). From the standpoint of analyte receptor sizes, streptavidin–biotin systems are both valid as models of antibody–antigen pairs, and biochemically amenable to controls for which antigen-antibody pairs are less well suited.

To summarize, it was found that HFET sensors respond to the engagement of biotinylated sensing channel surfaces by streptavidin (a negatively charged biotin binding protein) with reduced I_{sd}. Biotinylated analytes (biotinylated monokine induced by interferon gamma, bMIG, a positively charged, pro-inflammatory chemokine [**6**, **11**]) can then be bound to streptavidin on the HFET surface, and the HFET responds to bMIG binding with increased I_{sd}. The HFETs are n-type devices [**6**, **11**], so for each analyte, the direction of the responses (increasing/decreasing I_{sd}) were appropriate to the intrinsic charge of the analytes at experimental pH. Controls using biotin-saturated streptavidin and unbiotinylated MIG as analytes showed that the analytes must bind to the polymer film on the sensing surface to be detected by the HFET, as expected. The measured height of the interfacial protein-polymer films of the sensors

[**28**] showed that the necessity for interfacial binding for sensor detection of analyte reflected the fact that analytes must be within nanometre scale distance of the surface (less than 5 nanometres) to be detected by the HFET. Sensing exhibited an analyte dose response: signals were directly proportional to analyte concentrations [**11**].

These publications [**6**, **11**, **28**] and others [**9**, **14**, **15**, **17**, **18**, **32**] directly refute the classical immunoFET assessment with data. However, the classical assessment incorporates other features that were confirmed experimentally, most importantly being that HFET sensing signal to a fixed analyte concentration is inversely proportional to buffer salt content [**11**]. The results also ratified the classical assertion that nanometre scale charge-to-sensing surface distance is a critical determinant of signal magnitude [**6**, **11**, **24**, **28**].

The data are congruent with the re-assessment of the classical model in this paper. The classical model is incorrect when it asserts that it is infeasible to detect proteins in physiological buffers by FET, but entirely correct to suggest nanoscale analyte charge to FET surface distance determines the magnitude of FET sensing signal and that buffer ions can shield charges of bound analytes from the sensor.

3.5 Polymeric films and sensor operating properties

Structural differences between APTES and APDMES films substantially alter analyte binding properties. APDMES sites for derivatization (the terminal amines modified by Sulfo-NHS-biotin, and biotins bound by streptavidin) occur at roughly the same distance from the interface, whereas the amines (and biotins which are conjugated to the amines) are distributed throughout the APTES film (Fig. 5). This differential arrangement of silane amines and biotins conjugated to the amines should lead to differential streptavidin binding kinetics on the APTES and APDMES interfaces. ELISA analysis of streptavidin-HRP (horseradish peroxidase) binding to biotinylated APTES and APDMES films on AlGaN reveals this to be the case (Table 1).

For an APTES interface, ELISA reveals that streptavidin-HRP binding follows a biphasic course, with an initial rapid binding phase followed by a slower increase in signal over the duration of the experiment (Table 1). Streptavidin-HRP binding to APDMES interfaces exhibits different behaviour, featuring a rapid binding phase, similar to that seen with APTES films, after which further binding does not occur (Table 1). For both films, the initial rapid binding phase reflects binding of streptavidin-HRP to easily accessible biotin molecules on the film surface. In the case of APDMES, all biotins have similar accessibility as they are all at the surface of the film, and streptavidin binding proceeds rapidly until no further biotinylated surface is available (i.e. until the APDMES interface is biochemically saturated by streptavidin binding). In APTES films, there are biotins not only at the film surface, but distributed throughout the film (as are the terminal APTES amines in Fig. 5), so the initial phase of rapid binding is followed by an extended phase of diffusion-limited streptavidin–HRP binding as streptavidin–HRP molecules permeate the branched, biotinylated APTES network. Not surprisingly, the APTES interface binds substantially more streptavidin–HRP than can the APDMES film (Table 1).

The thicknesses of APTES and APDMES films differ by multiple nanometres: prior to biotinylation: the APDMES interface is half to one-third as thick as the APTES interface [**28**] (Table 1). In light of the critical importance of analyte charge-sensing surface proximity for FET detection of proteins [**1**, **3**, **5**, **6**, **10**, **11**], FET sensors with biotinyated APTES or APDMES interfaces should exhibit differential responses to analyte (streptavidin) in high-salt physiological buffers (PBS, 150 mM Na^+).

Streptavidin is a negatively charged protein at experimental pH (7.4), and since HFET charge carriers are electrons (the AlGaN HFET is an n-type device), binding of streptavidin reduces HFET I_{sd} ([**6**, **11**] Fig. 3). Electrical responses of HFETs with biotinylated APTES and biotinylated APDMES interfaces were determined by the current versus time method [**11**] after exposure of the HFETs to streptavidin in PBS.

HFETs with biotinylated APTES and APDMES interfaces respond to streptavidin binding with similar kinetics (see below), although the minimum concentrations of streptavidin detectable using the two interfacial layers are very different (Table 1). With a biotinylated APDMES interface, the minimal detectable concentration of streptavidin is four to six orders of magnitude lower than it is with a biotinylated APTES interface. The difference in HFET sensitivity reflects differences in structural and streptavidin binding characteristics of APTES and APDMES films on AlGaN. While the APTES interface binds more streptavidin per surface area than does the APDMES film (Table 1), sites for biotinylation and subsequent streptavidin binding (the amine groups of the silane monomers) are distributed throughout much of the thickness of the APTES film. In the thinner APDMES films, amines for biotinylation occur at a single, standardized distance from the sensing surface, determined by siloxane to amine length of APDMES monomers. It seems likely that APDMES-based interfaces bind sufficient streptavidin for HFET detection at lower streptavidin concentrations than do APTES-based interfaces because of the lesser film thickness of APDMES-based films (Table 1). This observation implies that some of the greater quantity

of streptavidin bound by APTES-based interfaces may be positioned too far away from the sensing channel surface to significantly influence sensor I_{sd}.

The magnitude of the difference in sensitivity of HFETs with APDMES versus APTES interfaces is remarkable. *In vacuo*, the sensitivity of FET response to proximal electric fields is expected to follow inversely the square of distance between charge and sensing channel [**39**], which could not account for the observed differences in sensitivity, given the small difference in interfacial film thickness between APTES and APDMES-based surface films. However, the results were generated in high osmolarity buffer, and the relationship between distance and I_{sd} is expected to follow a much higher exponential function under those circumstances [**39**]. While he does not fully describe how much higher he expects the exponential function describing distance between analyte charge and sensor surface to be in PBS (150 mM Na^+), Israelachvili [**39**] appears to be correct in saying that the function is much steeper in high-salt buffers than *in vacuo*. A manuscript further substantiating and detailing the empirically determined relationship between charge-sensing surface distance and sensor signal is in preparation [**40**].

The kinetics of response between HFET devices with APTES- and APDMES-based interfaces was similar, even though ELISA experiments indicate that the biotinylated APDMES interface biochemically saturates quickly, but the biotinylated APTES interface does not (Table 1). The electrical response reflects kinetics seen in ELISA experiments. Electrical characterization occurs entirely during the initial rapid pre-saturation streptavidin-binding phase that occurs with both silane films, so similar HFET response kinetics between devices with APTES- and APDMES-based interfaces are expected in this experiment. To avoid foreign body responses that accrue for long-term synthetic implants, the authors intend to expose sensors to tissue very transiently on a needle probe [**27**]. The observed response kinetics modelled those expected in use of the sensor in its planned clinical application.

In longer duration electrical characterization experiments, assuming similar streptavidin concentrations as used in ELISA (concentrations used in ELISA are substantially higher than used for electrical sensing), devices with biotinylated APDMES- and APTES-based interfaces would be expected to exhibit electrical response kinetics that emulate the differential streptavidin binding behaviour seen in ELISA assay, at least to the extent that the sensor electrical signal using the APDMES-based interfaces should cease to increase after the biotinylated APDMES film biochemically saturates with streptavidin. Since some of the streptavidin bound to the biotinylated APTES interface may contribute to sensor response to a lesser degree than does streptavidin bound to the biotinylated APDMES interface, it is unclear to what extent the sensor signal will parallel ELISA results for APTES films after the initial rapid binding phase is complete. While intriguing, the question has limited relevance to the planned use of the sensor in transplant biology, wherein assays will be carried out over a period of less than 100 s via a needle-mounted sensor probe.

3.6 FET hardware modification to support enhanced performance and commercial/clinical translation

To this point, consideration has focused primarily on treatments of finished HFET devices (oxidation, polymer interfacial layers, etc.) that potentially improve protein-sensor performance, although modification of the HFET device platforms themselves can enhance their performance as protein sensors. For instance, an electrical bias can be applied to the FET sensing channel via a reference electrode (commonly called a control gate). Under bias by a control gate, FET devices can be operated in different response regimes defined by the bias. Typically, FETs, including the HFETS used here [**6**, **11**], are operated in a linear response regime wherein I_{sd} changes linearly with the electrostatic potential induced by bound analytes. However, with a control gate, it is possible to bias the device to the subthreshold response regime, wherein I_{sd} changes logarithmically in response to bound analyte charge. Sensor sensitivity to analyte is thus expected to be orders of magnitude higher when the device is biased to the subthreshold regime than with an otherwise comparable device operating in the linear response regime.

The concept has been successfully applied to an AlGaN/GaN HFET hydrogen gas sensor. Under control gate bias to the exponential subthreshold response regime, HFET hydrogen sensors were three to four orders of magnitude more sensitive than comparable devices operating in the conventional linear response range [**41**]. Preliminary results with AlGaN/GaN protein sensors biased to the subthreshold regime by control gate also show significant sensitivity enhancement and are described elsewhere [**24**].

Protein sensors operating in biological environments are necessarily exposed to high osmolarity solutions. Permeation of ions into traditional silicon-based MOSFETs results in electrical instability of the MOSFET that can interfere with analyte sensing [**11**]. A central feature of AlGaN/GaN HFETs that allows stable operation in high-salt buffers (as will be encountered *in vivo*) is the impermeability of the AlGaN interface to mobile buffer ions. Despite this desirable feature, AlGaN/GaN HFETs are so costly that their translation to clinical devices may not be possible. It would be highly desirable to utilize a more economical architecture, such as silicon MOSFETS, if

such architectures could be adapted to use in high-salt environments.

It may be possible to produce barriers to ion permeation into the capacitance layer of silicon devices by deposition of alternative dielectric layers over their gate oxides. This might be accomplished economically by ALD, potentially rendering low-cost MOSFETs stable to buffer ion permeation-mediated drift. To demonstrate the feasibility of the approach, MOS capacitors are used here as convenient models of MOSFETs. Following exposure to a buffer, the presence of mobile ions such as sodium (Na^+) in the capacitor oxide can be demonstrated by bias temperature stress measurement (BTSM), wherein the application of a voltage bias at elevated temperatures leads to ion transport that shifts measurable voltages.

Silicon capacitors were made as described in section 2, and 100 nm aluminium oxide (Al_2O_3) high-K dielectrics were deposited by ALD to some of the capacitors. The as-grown oxide showed large positive fixed oxide charge with large frequency dispersion in C–V owing to interface states, which were remediated by annealing. The effective dielectric constant for the annealed Al_2O_3 layer was ∼8.5.

ALD-treated and annealed capacitors were incubated in PBS (150 mM Na^+) for 5 min (comparable to the current HFET protein detection experiments), after which a bias temperature stress measurement was performed (C–V measurement at 100 kHz). Then capacitors were heated to 200 °C, with a stress bias of 5 V for 10 min, and the samples were cooled to room temperature with the bias applied and the C–V measurement was repeated. The process was then repeated then for a −5 V stress voltage. Positive stress voltage at raised temperature is expected to push mobile ions (Na^+) in the oxide towards the oxide/semiconductor interface, concomitantly shifting the C–V curve to the left. On the other hand, negative stress bias moves mobile ions towards the gate electrode/oxide interface, shifting the C–V curve to the right. The flatband voltage shift, ΔV_{FB} determines the amount of mobile charge present in the oxide given by $Q_m = C_{ox}\Delta V_{FB}$, where C_{ox} is the accumulation capacitance.

The opposite behaviour was observed, indicating presence of charge injection into the oxide. A comparison of samples before and after PBS exposure show similar flat band voltage shifts with a small decrease in the flatband shift after incubation in PBS. The effect could be due to opposing effects of Na^+ ion and charge injection. To corroborate that interpretation, an alternative electrical characterization technique (triangular sweep method, TSM) was performed [**42**].

TSM utilizes a quasi-static C–V measurement at elevated temperatures (∼250 °C). TSM measures the charge flow in the oxide in response to a time-varying voltage and has a higher sensitivity than BTSM. TSM can detect mobile ion densities as low as $10^9\,cm^{-2}$. Initial TSM studies document significant Na^+ ion permeation after PBS incubation for ALD-untreated silicon capacitors (Fig. 6), corroborating the earlier conclusion that silicon FETs exhibited electrical drift after exposure to PBS as the result of Na^+ permeation of their SiO_2 capacitance layers [**6**, **11**].

BTSM and TSM analysis of identical MOS capacitors with a high-K Al_2O_3 dielectric deposited by ALD produced very different results. Capacitors with ALD-deposited Al_2O_3 layers exhibited no measurable shifts, indicating the absence of Na^+ permeation in these devices (data not shown). Work is currently proceeding to identify the minimal thickness and optimal composition/structure dielectric layer for Si-based immunoMOSFETs. Such devices would have costs of only pennies to dollars per unit, making them attractive candidates for commercial translation for clinical (and other) applications.

4 CONCLUSION

This paper describes/reviews a suite of optimization approaches that are being pursued concurrently for a planar immunoFET device. Many of the device/interface enhancements can most likely be introduced concurrently into FET sensors without compromising the beneficial effects that they individually provide in sensor function. Other optimizations might best be tuned to each other. For instance, specific AlGaN surface oxidation conditions, specific interfacial polymer films, and specific receptor protein molecules (not discussed here) may produce better sensor function only if they are incorporated together into a single sensor.

The classical assessment of immunoFET infeasibility is fundamentally flawed in the specific assumptions regarding protein charges, antibody flexibility, and antibody binding to surfaces and ignores the potential of engineering antibodies to adapt them to immunoFET use. However, the model was correct in asserting analyte charge–sensor surface distance plays a major role in determining sensor signal strength. In this limited sense, the data presented corroborate the classical model, and are consistent with Israelachvili's [**30**] further assessment that the function describing the distance/signal relationship in high-salt buffer is very steep in the nanoscale distance regime. There is an ongoing investigation of the distance/signal relationship using precise height interfacial components and standard analytes, and an effort to report further empirical confirmation of Israelachvili's speculation in the near future.

Many of the optimization approaches here have not reached final fruition. For instance, the 100 nm Al_2O_3 ALD layer shown here may not be optimal

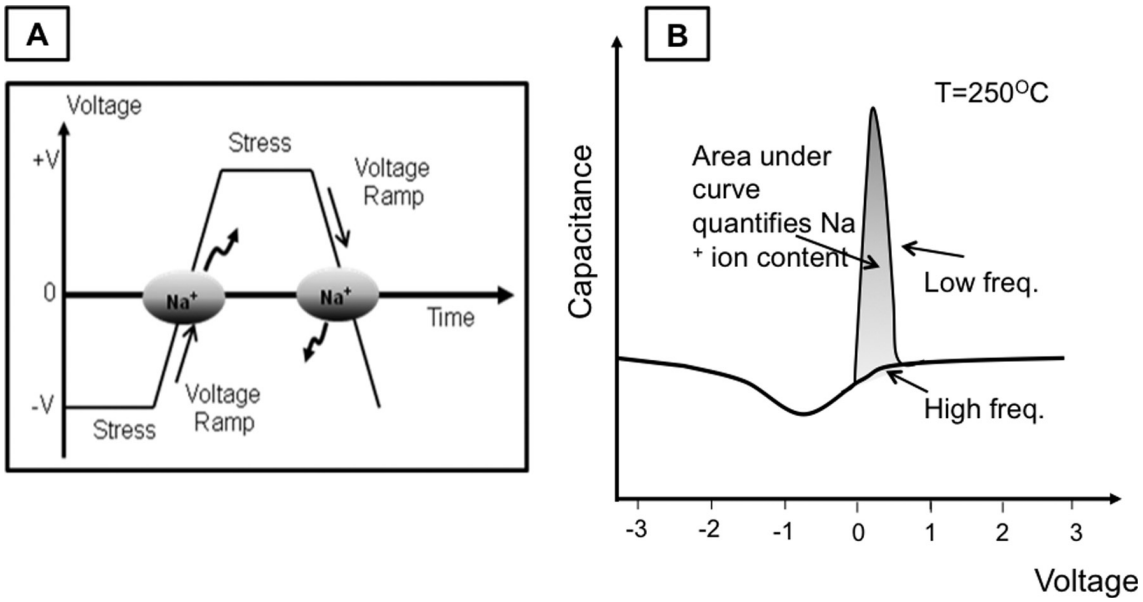

Fig. 6 Electrical analysis of MOS capacitors exposed to high osmolarity buffer (PBS) providing evidence of mobile ion (Na^+) permeation of device SiO_2 capacitance layer. (a) The 'triangular' voltage applied to the MOS capacitor at elevated temperature. Na^+ ion movement is detected in the *C*–*V* when the applied voltage changes polarity. (b) *C*–*V* curve measure at elevated temperature for TSM method. The peak in the low-frequency curve around 0 V is attributed to sodium ion movement within the SiO_2 interface. The area under the curve quantifies Na^+ ion content

from the standpoints of layer composition and thickness. Nonetheless, preliminary data from capacitors with such Al_2O_3 surfaces support the notion that ALD might mitigate ion permeation of silicon devices in biologic environments. The effect of ALD on FET protein sensor sensitivity also remains to be determined. However, there is reason to believe that the high-K dielectric layers could actually enhance sensitivity: higher effective dielectric constants increase induced electrostatic coupling and boost measurable signal. If sufficient sensitivity is retained by immunoMOSFETs made ion permeation resistant by ALD, then planar immunoFETs are not only feasible, but may also be economical enough to become real clinical tools.

In the case of the analyte under current investigation (monokine induced by interferon gamma, MIG [**6**, **11**]) the demonstration HFET (prior to any of the enhancements discussed in this paper) can detect analyte at concentrations occurring in severely inflamed tissue, but is two to three orders of magnitude too insensitive to detect MIG at concentrations found in normal (non-inflamed) tissue. However, using the HFET platform, considering observed sensitivity enhancements resulting from optimizations discussed here, planar immunoFETs would seem to be feasible as potential analytical tools, contrary to the classical analysis [**1**–**5**]. Final clinical and commercial translation may require moving away from the AlGaN/GaN HFET platform for purely pharmacoeconomic reasons. Nonetheless, the AlGaN/GaN HFET platform plays a pivotal role in establishing the feasibility of the technology. The data presented here, and in associated papers [**6**, **9**–**15**, **17**, **18**], suggest strongly that the objective of clinically useful immunoFETs may well be achievable.

ACKNOWLEDGEMENTS

This work was supported in part by award GRT00015533 from the National Science Foundation, awards from The Program for Homeland Security of the Ohio State University, and awards from the Institute for Materials Research of the Ohio State University.

REFERENCES

1 **Schöning, M. J.** and **Poghossian, A.** Recent advances in biologically sensitive field-effect transistors (BioFETs). *The Analyst*, 2002, **127**(9), 1137.
2 **Bergveld, P.** Development, operation, and application of the ion-sensitive field-effect transistor as a tool for electrophysiology. *IEEE Trans. Biomed. Engng*, 1972, **bme-19**(5), 342.
3 **Bergveld, P.** A critical evaluation of direct electrical protein detection methods. *Biosensors and Bioelectronics*, 1991, **6**(1), 55–72.
4 **Bergveld, P**. The future of biosensors. *Sensors & Actuators: A. Physical*, 1996, **56**(1–2), 65.

5 **Schöning, M. J.** and **Poghossian, A.** Bio FEDs (field-effect devices): state-of-the-art and new directions. *Electroanalysis*, 2006, **18**(19–20), 1893–1900.

6 **Shapiro, J. P., Gupta, S. K., Elias, M. A., Wen, X., Eteshola, E., Brillson, L., Lu, W.,** and **Lee, S. C**. Challenges in optimization of nanobiotechnological devices illustrated by partial optimization of a protein biosensor. In Proceedings of 2nd International Congress on *Nanobiotechology and nanomedicine*, 2007.

7 **Janeway, C. A., *et al*.** *Immunobiology: the immune system in health and disease*, fourth edition, 1999 (Taylor & Francis, New York).

8 **Abbas, A. K., Lichtman, A. H.,** and **Pober, J. S.** *Cellular and molecular immunology*, 1991 (Saunders, Philadelphia).

9 **Estrela, P., *et al*.** Label-free sub-picomolar protein detection with field-effect transistors. *Analyt. Chem.*, 2010, **82**(9), 3531–3536.

10 **Eteshola, E., *et al*.** Engineering functional protein interfaces for immunologically modified field effect transistor (ImmunoFET) by molecular genetic means. *J. R. Soc. Interface*, 2008, **5**(18), 123–127.

11 **Gupta, S., Elias, M., Wen, X., Shapiro, J., Brillson, L., Lu, W.,** and **Lee, S. C.** Detection of clinically relevant levels of protein analyte under physiologic buffer using planar field effect transistors. *Biosensors and Bioelectronics*, 2008, **24**(4), 505.

12 **Lud, S. Q., *et al.*** Field effect of screened charges: electrical detection of peptides and proteins by a thin-film resistor. *Chem. Phys. Chem.*, 2006, **7**(2), 379–384.

13 **Nair, P. R.** and **Alam, M. A.** Screening-limited response of nanobiosensors. *Nano Letters*, 2008, **8**(5), 1281–1285.

14 **Windbacher, T., Sverdlov, V.,** and **Selberherr, S.** Biotin-streptavidin sensitive BioFETs and their properties. *Biomed. Engng Syst. Technol.*, 2010, 85–95.

15 **Windbacher, T., *et al.*** Simulation of field-effect biosensors (BioFETs) for Biotin-streptavidin complexes. In Proceedings of the 29th International Conference on *Physics of semiconductors*, 2010, Rio de Janeiro, Brazil.

16 **Junghui, S.** and **Wu, L.** AlGaN/GaN Heterostructure field effect transistors for high temperature hydrogen sensing with enhanced sensitivity. In *Electron Devices Meeting (IEDM 2007)*, 2007 (IEEE International, New York).

17 **Baumgartner, O. E. O., Gös, W., Stimpfl, F., Windbacher, T.,** and **Selberherr, S.** *VISTA status report*, 2008 (Institute for Microelectronics, Vienna).

18 **Baumgartner, O. E. O., Gös, W., Stimpfl, F., Windbacher, T.**, and **Selberherr, S.** *VISTA status report*, 2009 (Institute for Microelectronics, Vienna).

19 **Lee, S .C., Bhalerao, K.,** and **Ferrari, M.** Object-oriented design tools for supramolecular devices and biomedical nanotechnology. *Ann. New York Acad. Sci.*, 2004, **1013** (The Coevolution of Human Potential and Converging Technologies), 110–123.

20 **Bhalerao, K. D., *et al*.** Nanodevice design through the functional abstraction of biological macromolecules. *Appl. Phys. Lett.*, 2005, **87**(14), 143902–3.

21 **Bhushan, B. *et al*.** Morphology and adhesion of biomolecules on silicon based surfaces. *Acta Biomaterialia*, 2005, **1**(3), 327–341.

22 **Bhushan, B., *et al*.** Nanoscale adhesion, friction and wear studies of biomolecules on silicon based surfaces. *Acta Biomaterialia*, 2006, **2**(1), 39–49.

23 **Lee, S. C., *et al*.** Protein binding on thermally grown silicon dioxide. *J. Vacuum Sci. Technol. B: Microelectronics Nanometer Structs*, 2005, **23**(5), 1856–1865.

24 **Wen, X. S. M. L., Gupta, S., Nicholson III, T. R., Lee, S. C.,** and **Lu, W.** Improved sensitivity of AlGaN/GaN field effect transistor biosensors by optimized surface functionalization. *IEEE Sensors J.*, 2010.

25 **Brillson, L. J.** *Surfaces and interfaces of electronic materials*, first edtion, 2010, pp. 93–145 (Wiley-VCH, Weinheim).

26 **Seah, M. P.** and **Dench, W. P.** Quantitative electron spectroscopy of surfaces. *Surface Interface Analysis*, 1979, **1**(2) 2–11.

27 **Gupta, S. *et al*.** 2010 Structures and tribological properties of protein/polymer films on oxidized AlGaN *J. Appl. Phys. D* (submitted).

28 **Bhushan, B., *et al*.** Nanoscale adhesion, friction and wear studies of biomolecules on silane polymer-coated silica and alumina-based surfaces. *J. R. Soc. Interface*, 2009, **6**(37) 719–733.

29 **Roach, P., Farrar, D.,** and **Perry, C. C.** Interpretation of protein adsorption: surface-induced conformational changes. *J. Am. Chem. Soc.*, 2005, **127**(22), 8168–8173.

30 **Ikeda, T., *et al*.** Oriented immobilization of antibodies on a silicon wafer using Si-tagged protein A. *Analyt. Biochemistry*, 2009, **385**(1), 132–137.

31 **Ikeda, T., *et al.*** Single-step affinity purification of recombinant proteins using the silica-binding Si-tag as a fusion partner. *Protein Expression and Purification*, 2009, **71**(1), 91–95.

32 **Kang, B. S., *et al*.** Electrical detection of immobilized proteins with ungated AlGaN/GaN high-electron-mobility transistors. *Appl. Phys. Lett.*, 2005, **87**(2), 023508–3.

33 **Kallury, K. M. R., Macdonald, P. M.,** and **Thompson, M.** Effect of surface water and base catalysis on the silanization of silica by (aminopropyl)alkoxysilanes studied by X-ray photoelectron spectroscopy and 13c cross-polarization/magic angle spinning nuclear magnetic resonance. *Langmuir*, 1994, **10**(2), 492–499.

34 **Howarter, J. A.** and **Youngblood, J. P.** Optimization of silica silanization by 3-aminopropyltriethoxysilane. *Langmuir*, 2006, **22**(26), 11142–11147.

35 **Wu *et al.*** Nanoscale depth resolved surface plasma oxidized AlGaN/GaN heterostructure for immuno-modified field effect transistors. *Journal of Vacuum Science and Technology B* (submitted) 2010 .

36 **Nissim, A.** Antibody fragments from a'single pot'phage display library as immunochemical reagents. *EMBO J.*, 1994, **13**(3), 692.

37 **Arbabi Ghahroudi, M., *et al.*,** Selection and identification of single domain antibody fragments from camel heavy-chain antibodies. *FEBS Lett.*, 1997, **414**(3), 521–526.

38 **Muyldermans, S., Cambillau, C.,** and **Wyns, L.** Recognition of antigens by single-domain antibody fragments: the superfluous luxury of paired domains. *Trends Biochem. Sci.*, 2001, **26**(4), 230–235.

39 Israelachvili, J. N. *Intermolecular and surface forces*, second edition, 1992 (Academic Press, London).
40 Gupta *et al.*, 2010b, Relationship between interfacial film morphology and immuno/bioFET sensitivity *Biosensors and Bioelectronics* (submitted).
41 Junghui, S. and **Wu, L**. Operation of Pt/AlGaN/GaN-heterojunction field-effect-transistor hydrogen sensors with low detection limit and high sensitivity. *Electron Device Lett., IEEE*, 2008, **29**(11), 1193–1195.
42 Schroder, D. K. *Semiconductor material and device characterization*, 2006 (Wiley-Interscience, New York).

APPENDIX

Notation

Abs	absorbance
C_{ox}	accumulation capacitance
d	depth
E_B	binding energy
E_k	photoelectron kinetic energy
h	Planck's constant
I_0	initial intensity
I_S	intensity of the substrate emissions
I_{sd}	current between source and drain terminals
Q_m	amount of mobile charge
ΔV_{FB}	flatband voltage shift
Θ	angle of photoelectron emission
λ	electron scattering length
ν	frequency